CrossMark

Tunable Multimode Plasmonic Filter Based on Side-Coupled Ring-Groove Joint Resonator

Kunhua Wen[1] · Yihua Hu[1] · Li Chen[1] · Jinyun Zhou[1] · Miao He[1] · Liang Lei[1] ·
Ziming Meng[1]

© Springer Science+Business Media New York 2016

Abstract A tunable multimode plasmonic filter is proposed by using a side-coupled ring-groove joint resonator. In addition to the integer resonance modes of the perfect ring resonator (RR), extra non-integer resonance modes are excited by adding a groove on the RR. According to the simulations with finite difference time domain method, it is investigated that two integer and two non-integer modes are obtained. When the groove is placed on the antinodes of the magnetic fields, the effective resonance lengths for the corresponding modes will be changed by the groove. In this case, one can linearly manipulate the wavelengths by changing the length of the groove. On the contrary, the wavelengths of the specific modes will be always fixed when the groove locates at the nodes of the modes. Compared to those perfect structured Fabry-Pérot (FP) resonators, this compact device can provide more channels and manipulate the wavelengths flexibly. Therefore, it may find widely applications in the on-chip optical signal processing area.

Introduction

Metal/dielectric integrated structures, which overcome the diffraction limit due to the surface plasmon polaritons (SPPs), can manipulate light in the nanoscale domain and thus receive considerable interest. Metal-dielectric-metal (MDM) and dielectric-metal-dielectric (DMD) structures are the two typical kinds of subwavelength structures. Especially, those MDM structures show great potential in the integrated photonic area [1–3], owing to the advantages of deep subwavelength confinement of light and easily manufacture process, which benefits from the promising fabrication technologies of focused ion beam, lithography, etching, and template methods [4–8]. A variety of plasmonic devices based on MDM waveguides have been proposed and demonstrated, such as filters [9–12], sensors [13–17], couplers [18–20], and so on. As one of those impressive MDM structures, RR, where local SPP resonance will arise, has attracted lots of attention [21–24]. It should be noted that FP resonance is a common and basic effect in these resonators [25, 26]. Through the FP effect, plasmonic filters were firstly achieved by using single side-coupled or end-coupled MDM resonator, and then, electromagnetic induced transparency phenomenon and Fano resonance were observed by using different RR arrangements [27, 28]. However, limited by the FP effect, there will be only one or two channels in a large wavelength range. Specifically, the wavelengths of the resonance modes are fixed by the effective lengths of the resonators and meet the proportion relation of $1 : 1/2 : 1/3 : \cdots$. This character may be not suitable for the development of on-chip multi-channel filtering.

In this letter, a plasmonic tunable multi-channel filter is proposed based on the RR structure. In addition to the conventional modes in the RR, two extra resonance modes are excited by adding a groove on the side-coupled RR. Four resonance modes in a certain wavelength range are obtained. According to the magnetic field distributions of the modes in the resonator, the position of the groove is an important factor to affect the wavelengths of the forbidden bands. When the groove locates at the antinodes of the magnetic fields, red shift will occur for the band-gap wavelengths by increasing the length of groove. Instead, the mode wavelength is immune to the groove when it is placed at the nodes. The performance

✉ Kunhua Wen
khwen@gdut.edu.cn

[1] School of Physics and Optoelectronic Engineering, Guangdong University of Technology, Guangzhou, Guangdong 510006, China

of the proposed structure is investigated by using the finite difference time domain method (FDTD) method.

Analyses and Results

The schematic of the proposed structure is illustrated in Fig. 1, which shows that a side-coupled RR is placed above a MDM bus waveguide. Figure 1a is the cross-section (x-y plane) schematic, and the Fig. 1b is the perspective view which can show more detailed design of the 3D structure. However, 2D FDTD simulations, which have been widely demonstrated to have the comparable accuracy with the 3D simulations but save much more running time, are employed in this paper. Therefore, the parameter setup of the structure is mainly based on Fig. 1a, and the length in z-axis is ignored. A groove locates at the right side of the RR with an angle θ, which is between the groove and y-axis direction. In the following, θ is used to define the position of the groove and is firstly considered as $\theta = 90^\circ$. It is well known that the perfect ring can perform as an FP resonator, and the resonance modes should satisfy the condition:

$$\frac{2\pi \mathrm{Re}(n_{eff})}{\lambda} L_{eff} + \Delta\phi = 2m\pi, \quad m$$
$$= 1, 2, 3, \cdots \quad (1)$$

where D is the width of the waveguide, $L_{eff} = \pi(R + r)$ is the effective resonance length, R and r are the outer radius and inner radius, respectively, $\Delta\phi$ is the phase change in the resonator, m stands for the integer resonance mode, and $\mathrm{Re}(n_{eff})$ is the real part of effective index n_{eff}, which can be obtained by the dispersion equation of the TM mode in the waveguide [29]:

$\varepsilon_d k_m + \varepsilon_m k_d \tanh(-jk_d D / 2) = 0$, where $k_{d,m} = \sqrt{\varepsilon_{d,m} k_0^2 - \beta^2}$ and $\varepsilon_{d, m}$ are the transverse propagation constant and permittivity in dielectric and metal, respectively. It should be noted that TE surface plasmon waves do not generally exist in planar metal-dielectric structures, since continuity of Ez forbids charge accumulation at the interface. This physical mechanism and phenomenon have been deeply analyzed by J. A. Dionne [29]. Therefore, we only consider the TM mode in the MIM waveguide and obtain the effective refractive index from the dispersion equation. According to Eq. (1), the transmission-band-gap wavelengths should approximately follow the condition: $\lambda_1 : \lambda_2 = 1 : 1/2$, where λ_1 and λ_2 are the wavelengths of the 1st-order and 2nd-order resonance modes of M_1 and M_2, respectively. After adding a groove to the RR, the resonance condition will be changed. Parts of SPPs will be captured into the groove, and thus, extra non-integer modes will be excited. In this case, the new generated modes, which are called mode $M_{(m + 1/2)}$, will no longer satisfy the phase condition in Eq. (1). Besides, when the groove locates at the antinodes of the magnetic fields of the original integer modes, SPPs will also be captured into the groove, and then the effective resonance length L_{eff} is changed. As such, the wavelengths of the corresponding modes will be linearly affected by the length of the groove. Otherwise, the wavelengths of the resonance modes should be immune to the groove when it is placed at the nodes. Based on this characteristic, one can easily manipulate the wavelengths of the specific modes by changing the position and the length of the groove.

In the following, FDTD method with PML layer is used to investigate the performance of the proposed structure. The source and the grid size are defined as plane wave and 5 × 5 nm, respectively. The metal and dielectric are air and silver, whose optical constants are obtained from the experiment [30]. The detailed parameters are defined as follows: the widths of the bus MDM waveguide and the groove $D = 50$ nm, the coupling distance $s = 15$ nm, the inner radius $r = 150$ nm, the outer radius $R = 200$ nm, and the angle $\theta = 90^\circ$.

The transmission spectrum of the perfect RR is shown in Fig. 2(a), where two integer resonance modes of M_1 and M_2 arise at the wavelengths of 1544.2 and 779.6 nm, respectively. Through the magnetic field distributions in Fig. 3(a), (b) for M_2 and M_1, it can be clearly seen that even antinodes are distributed along the RR (i.e., four in Fig. 3(a) and two in Fig. 3(b)), respectively. Interestingly, the magnetic field intensities for the two modes share the same nodes at the left or right side of the RR. Therefore, we firstly place the groove on the right side of the RR (i.e., $\theta = 90^\circ$) to investigate the performance. By setting $L = 100$, 150, and 200 nm, the transmission spectra are shown in Fig. 2(b)–(d), respectively. In addition to the integer
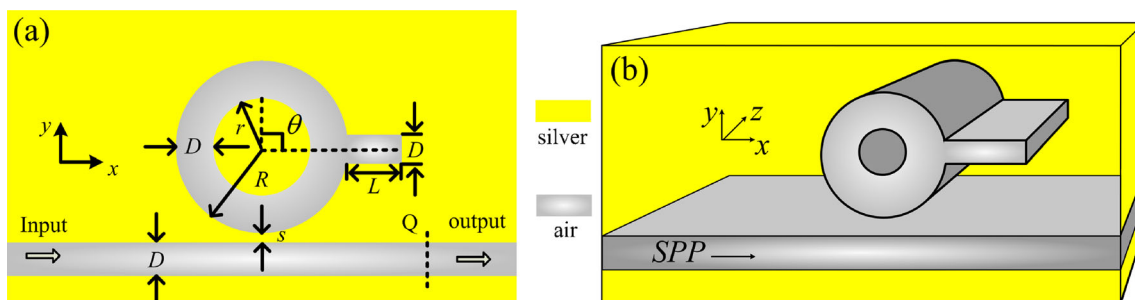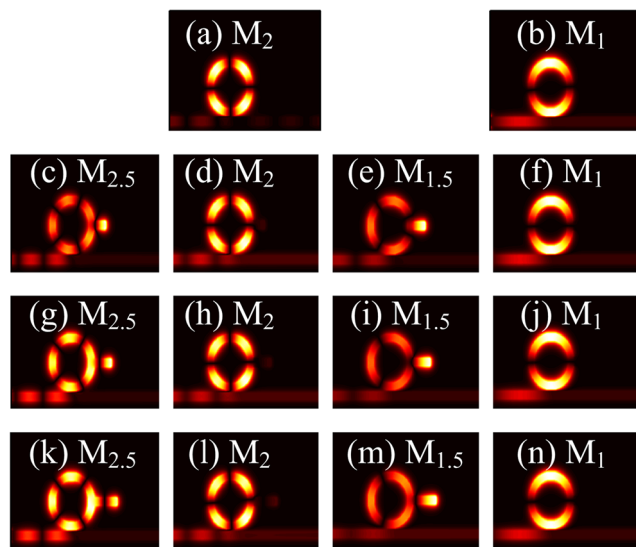

Fig. 1 Schematic of ring resonator with a groove. (a) x-y plane. (b) Perspective view
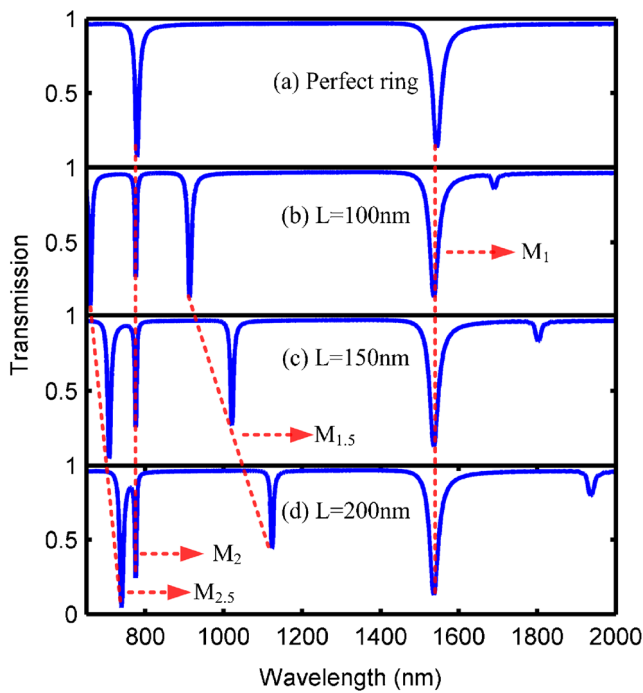
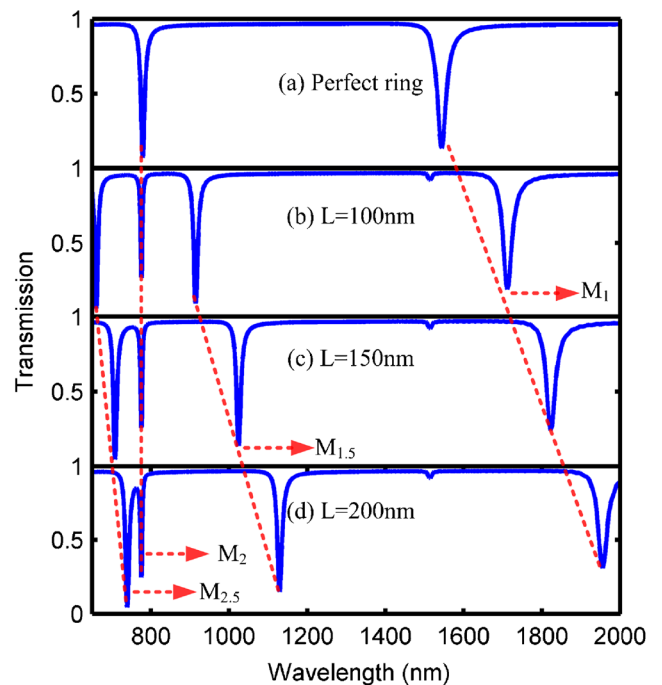**Fig. 2** Transmission spectra: *(a) perfect ring, (b)–(c) with $\theta = 90^o$*

resonance modes of $M_{1, 2}$, non-integer modes of $M_{1.5}$ and $M_{2.5}$ are excited, and thus four transmission band gaps are obtained. Figure 3(c)–(n) shows the magnetic field intensity distributions of $M_{1, 1.5, 2, 2.5}$ in detail. Obviously, the groove locates at the nodes of $M_{1, 2}$, and thus none of SPPs are distributed in the groove (Fig. 3(d), (f), (h), (j), (l), (n)). That is to say the modes $M_{1, 2}$ are immune to the length variation of the groove; therefore, the wavelengths of $M_{1, 2}$ are always uniform as 1544.2 and 779.6 nm (see the red-dotted line in Fig. 2(b)–(d)), respectively. On the contrary, the wavelengths of $M_{1.5, 2.5}$ can be linearly
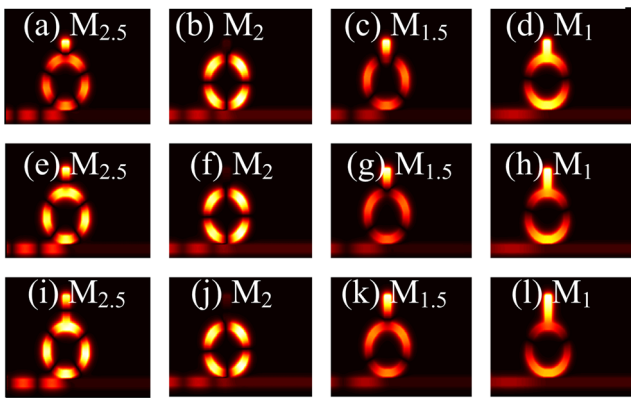
manipulated by changing L, as illustrated in Fig. 2(b)–(d) with red-dotted line. More details can be found in the magnetic field intensity distributions at the dip wavelengths in Fig. 3(c), (e), (g), (i), (k), (m). In this case, SPPs for $M_{1.5, 2.5}$ are captured and distributed in the groove, leading to the transform of the effective resonance length. Therefore, the wavelengths of $M_{1.5, 2.5}$ have red shift by increasing L. Generally, for the perfect ring structure, if the radius of the ring is increased, the wavelengths of both integer modes will red shift, but no new modes will be generated. However, there are four modes, including two integer modes and two extra generated non-integer modes, that are obtained by adding a groove.

Moreover, though the magnetic field intensity distributions in Fig. 3(a), we can see that the node for M_2 and the antinode for M_1 also have the same region at the top of the RR (i.e., $\theta = 0^o$), where the groove is placed to further investigate the performance. During the FDTD simulations, the parameters are the same as that in Fig. 2. The transmission spectra in Fig. 4 show that four resonance modes of $M_{1, 1.5, 2, 2.5}$ are also achieved. Compared to the wavelengths illustrated with red-dotted line, the wavelengths of modes $M_{1, 1.5, 2.5}$ are increased by changing the length of the groove, while the one of mode M_2 remains unchanged. The results agree well with the analysis above since the groove stands at the node of M_2 and the anti-nodes of $M_{1, 1.5, 2.5}$. The details of the magnetic field intensity distributions are shown in Fig. 5. It can be clearly seen that there is none of SPP energy in the groove for M_2 (Fig. 5(b), (f), (j)). This is completely different from the results of $M_{1, 1.5, 2.5}$ whose magnetic field intensities almost reach maximum in the groove (Fig. 5(a), (c), (d), (e), (g), (h), (i), (k), (l)).


Fig. 3 Magnetic field intensity distributions of modes $M_{1, 1.5, 2, 2.5}$: *(a) and (b) for perfect ring, (c)–(f) for L = 100 nm, (g)–(j) for 150 nm, and (k)–(n) for 200 nm, respectively*

**Fig. 4** Transmission spectra: *(a) perfect ring, (b)–(c) with $\theta = 0^o$*

Fig. 5 Magnetic field intensity distributions of modes $M_{1, 1.5, 2, 2.5}$ with $\theta = 0^o$: *(a)–(d) for L = 100 nm, (e)–(h) for 150 nm, and (i)–(l): 200 nm, respectively*

Figure 6 provides the more specific details about the wavelength variations of $M_{1, 1.5, 2, 2.5}$ with respect to the length L of the groove. In Fig. 6(a) with $\theta = 90^o$, the linear proportion between the wavelengths of $M_{1.5, 2.5}$ and L is further investigated by changing L from 100 to 220 nm with a step of 10 nm, while the ones of $M_{1, 2}$ always stays consistent. Besides, in Fig. 6(b) with $\theta = 0^o$, it is also confirmed that the wavelengths of $M_{1, 1.5, 2.5}$ increase linearly with L, except for the mode M_2. Therefore, one can flexibly design the wavelengths of the resonance modes by changing the position and the length of the groove.

In the following, the width of the RR and the length of the groove are fixed as 50 and 150 nm, respectively, and the outer radius R is changed to be 210, 220, and 230 nm to find out more characteristics. Obviously, four resonance modes can also be effectively excited due to the influence of the groove, as shown in the transmission spectra in Fig. 7. One can observe that all the wavelengths of the four band gaps have linearly red shift by increasing R. As such, it is concluded that the non-
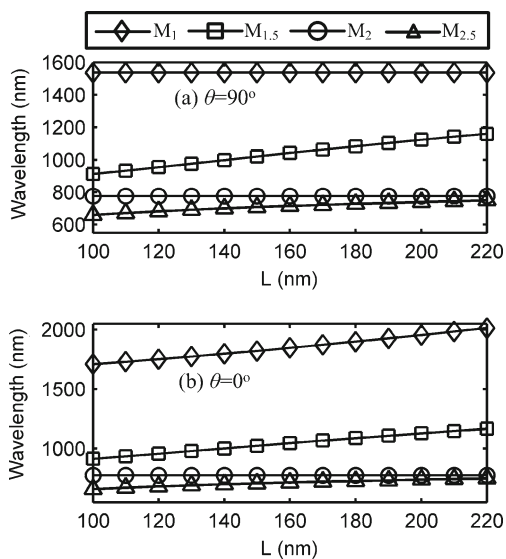
Fig. 6 The wavelength variations of $M_{1, 1.5, 2, 2.5}$ with respect to the length of the groove. *(a) $\theta = 90^o$, (b) $\theta = 0^o$*
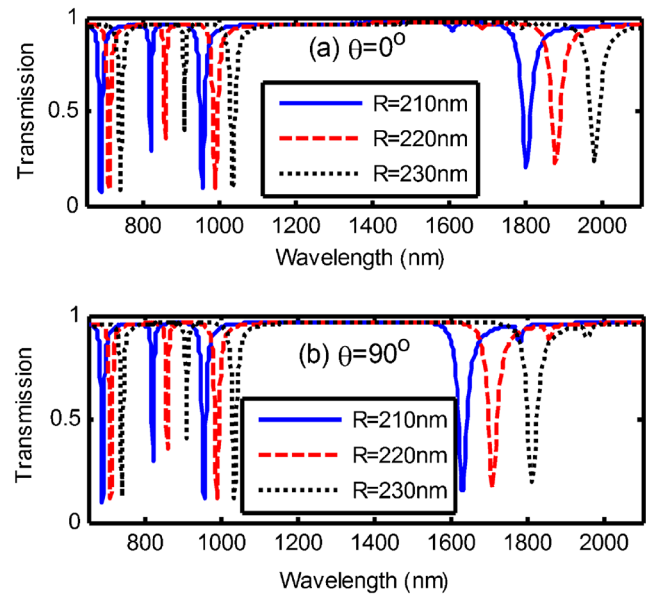
Fig. 7 Transmission spectra with different outer radius: *(a) $\theta = 0^o$, (b) $\theta = 90^o$*

integer modes can be equally excited in different RRs as well, and the wavelengths for all the modes can also be manipulated by the radius. This is another important characteristic to flexibly design the device with preferred performances.

Conclusion

Multiple resonance modes have been achieved by using the side-coupled RR system. In addition to the integer resonance modes of those FP resonators, non-integer modes were effectively excited by adding a groove on the RR. The simulation based on FDTD method demonstrated that the position of the groove would significantly affect the wavelengths of the modes. When the groove was placed on the antinodes of the modes, the wavelengths had linearly proportion with the length of groove. Otherwise, the wavelengths were fixed when the groove located on the nodes. Besides, it was investigated that the wavelengths of all the modes could also be manipulated by changing the radius of the RR. One may benefit from this characteristic, since it made the filter design more flexible and the resonance wavelength tunable. This kind of RR filter could find widely applications in the integrated optical circuits and optical system.

References

1. Gao H, Shi H, Wang C, Du C, Luo X, Deng Q, Lv Y, Lin X, Yao H (2005) Surface plasmon polariton propagation and combination in Y-shaped metallic channels. Opt Express 13(26):10795–10800
2. Bozhevolnyi SI, Volkov VS, Devaux E, Laluet JY, Ebbesen TW (2006) Channel plasmon subwavelength waveguide components including interferometers and ring resonators. Nature 440(7083):508–511
3. He ZH, Li HJ, Zhan SP, Li BX, Chen ZQ, Xu H (2015) Oscillator model analysis for slow-light in bright-dark-dark wavelength systems. IEEE Photon Lett 27(22):2371–2374
4. Matsuzaki Y, Okamoto T, Haraguchi M, Fukui M, Nakagaki M (2008) Characteristics of gap plasmon waveguide with stub structures. Opt Express 16(21):16314–16325
5. Halpern AR, Corn RM (2013) Lithographically patterned electrode-position of gold, silver, and nickel nanoring arrays with widely tunable near-infrared plasmonic resonances. ACS Nano 7(2):1755–1762
6. Lehr D, Dietrich K, Helgert C, Käsebier T, Fuchs HJ, Tünnermann A, Kley EB (2012) Plasmonic properties of aluminum nanorings generated by double patterning. Opt Lett 37(2):157–159
7. Bayati M, Patoka P, Giersig M, Savinova E (2010) An approach to fabrication of metal nanoring arrays. Langmuir 26(5):3549–3554
8. Cai Y, Li Y, Nordlander P, Cremer P (2012) Fabrication of elliptical nanorings with highly tunable and multiple plasmonic resonances. Nano Lett 12(9):4881–4888
9. Bahadori M, Eshaghian A, Hodaei H, Rezaei M, Mehrany K (2013) Analysis and design of optical demultiplexer based on arrayed plasmonic slot cavities: transmission line model. IEEE Photon Technol Lett 25(8):784–786
10. Wen KH, Hu YH, Chen L, Zhou JY, Lei L, Guo Z (2014) Design of an optical power and wavelength splitter based on subwavelength waveguides. J Lightwave Technol 32(17):3020–3026
11. Zhang Z, Shi F, Chen Y (2015) Tunable multichannel plasmonic filter based on coupling-induced mode splitting. Plasmonics 10(1):139–144
12. Deng Y, Cao GT, Wu YW, Zhou XQ, Liao WH (2015) Theoretical description of dynamic transmission characteristics in MDM waveguide aperture-side-coupled with ring cavity. Plasmonics 10(6):1537–1543
13. Lu H, Liu XM, Mao D, Wang GX (2012) Plasmonic nanosensor based on Fano resonance in waveguide-coupled resonators. Opt Lett 37(18):3780–3782
14. Chen Z, Yu L, Wang LL, Duan GY, Zhao YF, Xiao JH (2015) A refractive index nanosensor based on Fano resonance in the plasmonic waveguide system. IEEE Photon Lett 27(16):1695–1698
15. Chen Z, Yu L, Wang LL, Duan GY, Zhao YF, Xiao JH (2015) Sharp asymmetric line shapes in a plasmonic waveguide system and its application in nanosensor. J Lightwave Technol 33(15):3250–3253
16. Wen KH, Yan LS, Pan W, Luo B, Guo Z, Guo YH, Luo XG (2014) Electromagnetically induced transparency-like transmission in a compact side-coupled T-shaped resonator. J Lightwave Technol 32(9):1701–1707
17. Li BX, Li HJ, Zeng LL, Zhan SP, He ZH, Chen ZQ, Xu H (2015) High sensitivity sensing based on plasmon induced transparency. IEEE Photon J 7(5):4801207
18. Lee TW, Gray S (2005) Subwavelength light bending by metal slit structures. Opt Express 13(24):9652–9659
19. Wahsheh RA, Lu Z, Abushagur MAG (2009) Nanoplasmonic couplers and splitters. Opt Express 17(21):19033–19040
20. Bavil MA, Zhou Z, Deng Q (2013) Active unidirectional propagation of surface plasmons at subwavelength slits. Opt Express 21(14):17066–17076
21. Chen J, Li YD, Chen ZQ, Peng JY, Qian J, Xu J, Sun Q (2014) Tunable resonances in the plasmonic split-ring resonator. IEEE Photon J 6(3):1–6
22. Wen KH, Hu YH, Chen L, Lei L, Guo Z (2014) Single/multiple-mode-selection optical nanofilters based on end-coupled split-ring resonators. Appl Opt 53(19):4158–4163
23. Li Q, Wang T, Su YK, Yan M, Qiu M (2010) Coupled mode theory analysis of mode-splitting in coupled cavity system. Opt Express 18(8):8367–8382
24. Wen KH, Hu YH, Chen L, Zhou JY, Lei L, Meng ZM (2016) Plasmonic bidirectional/unidirectional wavelength splitter based on metal-dielectric-metal waveguides. Plasmonics 1(1):71–77
25. Hu FF, Yi HX, Zhou ZP (2011) Band-pass plasmonic slot filter with band selection and spectrally splitting capabilities. Opt Express 19(6):4848–4855
26. Zhang Q, Huang XG, Lin XS, Tao J, Jin XP (2009) A subwavelength coupler-type MIM optical filter. Opt Express 17(9):7549–7555
27. Chen Z, Song XK, Jiao RZ, Duan GY, Wang LL, Yu L (2015) Tunable electromagnetically induced transparency in plasmonic system and its application in nanosensor and spectral splitting. IEEE Photon J 7(6):1–8
28. Xia XS, Wang JC, Zhang F, Hu ZD, Liu C, Yan X, Yuan L (2015) Multi-mode plasmonically induced transparency in dual coupled graphene-integrated ring resonators. Plasmonics 10(6):1409–1415
29. Dionne JA, Sweatlock LA, Atwater HA (2006) Plasmon slot waveguides: towards chip-scale propagation with subwavelength-scale localization. Phys Rev B 73(3):035407
30. Johnson PB, Christy RW (1972) Optical constants of the noble metals. Phys Rev B 6(12):4370–4379